https://doi.org/10.5194/egusphere-2026-3534
Preprint. Discussion started: 20 July 2026

Green Above, Dry Below: Satellite Multi-Indices Reveal Contrasting Drought Trajectories Across the Tekeze Basin (2000–2025)

Bedasa Asefa Jinfessa[1,2,3], Jianjun Zhao[1,2,], Hongyan Zhang[1,2], Zhengxiang Zhang[1,2], Xiaoyi Guo[1,2], Mebrahtom Zerom Gebreyesus[1,2,4], Yosef Ermiyas Bergene[1] , Andeptop Sule[1]*

1 Key Laboratory of Geographical Processes and Ecological Security in Changbai Mountains, Ministry of Education, School of Geographical Sciences, Northeast Normal University, Changchun 130024, China;

2 Urban Remote Sensing Application Innovation Center, School of Geographical Sciences, Northeast Normal University, Changchun 130024, China;

3 Department of Geodesy and Geodynamics, Space Science and Geospatial Institute, Addis Ababa, 597, Ethiopia

4 Department of Geography, College of Business and Social Sciences, National Higher Education and Research Institute, Adi Keih, Eritrea

** Corresponding author E-mail address: zhaojj662@nenu.edu.cn (J.Zhao);*

Research Highlights

• Seven satellite-derived drought indices integrated over Tekeze Basin (2000-2025)

• Vegetation indices show positive trends (71-86%) while soil moisture declines

• Northern Tekeze sub-basin identified as a persistent multi-dimensional drought hotspot

• TCI-VCI correlation reaches r = 0.97; TVDI-VHI reaches r = -0.97 in peak season

• Multi-index framework reveals decoupling masked by single-index monitoring

https://doi.org/10.5194/egusphere-2026-3534
Preprint. Discussion started: 20 July 2026

Abstract

Drought is one of the most pervasive and damaging climate-related hazards in the Horn of Africa, with profound impacts on agricultural productivity, water resources, ecosystem functioning, and socioeconomic development. The Tekeze Basin of northern Ethiopia is particularly vulnerable due to its high rainfall variability, recurrent dry spells, and dependence on rain-fed agriculture. Although numerous drought studies have been conducted in Ethiopia, few have simultaneously integrated vegetation, thermal, soil moisture, precipitation, and surface water indicators to provide a comprehensive assessment of drought dynamics. This study presents a multi-dimensional spatiotemporal analysis of drought conditions in the Tekeze Basin (2000–2025) using seven satellite-derived drought indices: the Vegetation Condition Index (VCI), Temperature Condition Index (TCI), Vegetation Health Index (VHI), Temperature Vegetation Dryness Index (TVDI), Soil Moisture Condition Index (SMCI), Precipitation Condition Index (PCI), and Normalized Difference Water Index (NDWI). The indices were derived from MODIS, soil moisture, and CHIRPS precipitation datasets. Long-term pixel-wise temporal trends were assessed using the non-parametric Mann-Kendall (MK) test and Sen's slope estimator across the growing season (April–September), while inter-index relationships were examined through monthly Pearson correlation analysis. Results reveal that VCI, TCI, VHI, and NDWI exhibited predominantly positive trends over the study period (71.5–86.4% positive spatial coverage), indicating general improvement in vegetation and water conditions across most of the basin. In contrast, TVDI and SMCI showed dominant negative trends (82.2% and 55.3% negative coverage, respectively), indicating increasing land-surface dryness and declining soil moisture, particularly in the basin interior and lowlands. PCI displayed spatially heterogeneous patterns (54.7% negative coverage), signaling progressive precipitation deficits in the northern sub-basin. Monthly correlation analysis revealed strong positive relationships between TCI and VCI ($r = 0.48$–0.97) and strong negative relationships between TVDI and VHI ($r = -0.54$ to -0.97) across all months. SMCI and PCI showed strengthening positive intercorrelations during the peak rainy season (June–September). The contrasting trajectories observed between vegetation-based indicators and soil moisture-related indices suggest a potential decoupling between vegetation response and underlying hydrological conditions. These findings demonstrate the value of multi-index remote sensing approaches for capturing the complex and multidimensional nature of drought and provide important scientific evidence for drought early warning, water resource management, and climate adaptation planning in northern Ethiopia.

Keywords: Drought Monitoring; Spatiotemporal Analysis; Growing Season; Remote sensing; Tekeze Basin;

1. Introduction

Drought is a complex and slowly developing natural hazard that affects more people globally than any other climate-related disaster and causes substantial economic, environmental, and social losses (Wilhite, 2000; Sheffield and Wood, 2011). Unlike sudden-onset hazards such as floods and earthquakes, drought evolves gradually and manifests through multiple interconnected processes, including precipitation deficits, soil moisture depletion, vegetation stress, reduced streamflow, and declining water availability. These impacts are particularly severe in semi-arid and arid regions where livelihoods depend heavily on rain-fed agriculture and natural resources (Dai, 2013; Masih et al., 2014).

https://doi.org/10.5194/egusphere-2026-3534
Preprint. Discussion started: 20 July 2026

The Horn of Africa is recognized as one of the world's most drought-prone regions, experiencing frequent drought episodes driven by climate variability, changing atmospheric circulation patterns, and increasing climate extremes (Funk et al., 2015; Haile et al., 2020). Ethiopia has experienced numerous severe drought events over recent decades, resulting in widespread crop failures, livestock losses, food insecurity, and socioeconomic disruption (Bewket and Conway, 2007; Viste et al., 2013). The country's rainfall regime is strongly influenced by the Inter-Tropical Convergence Zone (ITCZ), Indian Ocean sea-surface temperature variability, and complex topographic conditions, which contribute to pronounced spatial and temporal rainfall variability (Diro et al., 2011; Seleshi and Zanke, 2004). Among Ethiopia's major river basins, the Tekeze Basin is particularly vulnerable because of its semi-arid climate, recurrent rainfall deficits, land degradation, and strong dependence on seasonal precipitation for agricultural production and water resources (Nyssen et al., 2004; Gebremicael et al., 2013; Tesfaye et al., 2017).

Reliable drought monitoring is essential for effective drought preparedness, early warning, and resource management. Traditional drought indicators such as the Standardized Precipitation Index (SPI) and Palmer Drought Severity Index (PDSI) have been widely applied for drought assessment and operational monitoring (Palmer, 1965; McKee et al., 1993). Although these indices effectively characterize meteorological drought conditions, they do not directly capture vegetation stress, soil moisture dynamics, land surface thermal conditions, or changes in surface water availability that collectively determine drought impacts on ecosystems and agriculture. Consequently, increasing attention has been directed toward remote sensing approaches that provide spatially continuous observations of drought-related variables over large geographic areas (AghaKouchak et al., 2015; Zhang et al., 2017).

Advances in satellite remote sensing have enabled the development of numerous drought indicators representing different components of the land-atmosphere system. Vegetation-based indices such as the Vegetation Condition Index (VCI) and Vegetation Health Index (VHI) quantify vegetation stress and productivity (Kogan, 1990; Kogan, 1997). The Temperature Condition Index (TCI) reflects thermal stress associated with drought conditions (Kogan, 1995), whereas the Temperature Vegetation Dryness Index (TVDI) provides information on land-surface dryness through vegetation-temperature relationships (Sandholt et al., 2002). Soil Moisture Condition Index (SMCI) characterizes moisture availability within the root zone (Du et al., 2013), while the Precipitation Condition Index (PCI) represents meteorological drought conditions based on rainfall variability (Rhee et al., 2010). The Normalized Difference Water Index (NDWI) provides additional information on vegetation water content and surface moisture conditions (Gao, 1996). Because each index captures a different aspect of drought, no single indicator can adequately represent the full complexity of drought processes.

Recent studies have increasingly demonstrated the advantages of integrating multiple drought indicators to improve drought characterization and monitoring accuracy (Yao et al., 2020; Ayana et al., 2022; Woldesenbet et al., 2023). Multi-index frameworks are particularly valuable in environmentally heterogeneous regions where meteorological, agricultural, and hydrological drought conditions may evolve differently across space and time. Despite growing interest in multi-dimensional drought assessment, comprehensive long-term studies integrating vegetation, temperature, soil moisture, precipitation, and water-related indicators remain limited in Ethiopia. Existing drought investigations in northern Ethiopia have primarily focused on individual drought indicators, short analysis periods, or localized study areas, leaving significant uncertainty regarding the interactions among different drought dimensions at the basin scale.

https://doi.org/10.5194/egusphere-2026-3534
Preprint. Discussion started: 20 July 2026

The Tekeze Basin represents a critical case study for advancing drought monitoring in Ethiopia because of its high climatic variability, ecological sensitivity, and socioeconomic importance. The basin encompasses diverse topographic and climatic conditions that may produce substantial spatial heterogeneity in drought responses. Furthermore, the agricultural growing season extending from April to September, including the Belg and Kiremt rainfall periods, is crucial for crop production, water availability, and rural livelihoods throughout the basin (Segele and Lamb, 2005; Conway et al., 2009). Understanding drought dynamics during this period is therefore essential for strengthening drought risk management and adaptation planning.

Against this background, this study presents a comprehensive multi-index assessment of drought dynamics in the Tekeze Basin during the growing season from 2000 to 2025. By integrating seven satellite-derived drought indices representing vegetation condition, thermal stress, soil moisture status, precipitation variability, and surface water conditions, the study seeks to provide a more complete understanding of drought evolution than can be achieved through individual indicators alone. Particular attention is given to identifying potential divergences among drought dimensions, including situations in which vegetation conditions improve while underlying soil moisture and hydrological conditions deteriorate.

The specific objectives of this study are to: (1) characterize the spatial and temporal patterns of drought across the Tekeze Basin during the growing season using seven satellite-derived drought indices; (2) quantify long-term drought trends through pixel-wise Mann–Kendall trend analysis and Sen's slope estimation; and (3) evaluate interrelationships among vegetation, thermal, soil moisture, precipitation, and water-related drought indicators using monthly correlation analysis. The findings are expected to contribute to improved drought monitoring frameworks, support operational drought early warning systems, and provide scientific evidence for climate-resilient water and agricultural management in northern Ethiopia.

2. Data and Methods

2.1 Study Area

The Tekeze Basin (approximately 36°–40°E, 11.5°–15°N) is located in northern and northwestern Ethiopia and covers an area of approximately 82,000 km² (Figure 1). The basin drains northward into Sudan, where the Tekeze River merges with the Setit and subsequently joins the Atbara River before discharging into the Nile. The climate of the Tekeze Basin is predominantly semi-arid to arid, with mean annual rainfall ranging from less than 300 mm in the northern and eastern lowlands to over 1,200 mm in the western highland escarpments. Rainfall is highly seasonal, concentrated in two distinct wet seasons: the short Belg rains (March–May, contributing 10–25% of annual rainfall) and the main Kiremt rainy season (June–September), contributing 60–80% of annual rainfall (Seleshi and Zanke, 2004; Segele and Lamb, 2005; Diro et al., 2011; Nicholson, 2018). Mean annual temperatures range from approximately 12°C in the western highlands to more than 34°C in the Afar lowlands. Land cover in the basin includes rainfed subsistence agriculture (predominantly in the highlands and mid-elevations), semi-arid shrubland and open woodland (intermediate zones), seasonal and perennial riverine vegetation along major tributaries, and bare or sparsely vegetated surfaces in the Afar lowlands (Nyssen et al., 2004; Gebre et al., 2015). Ongoing watershed rehabilitation and conservation programs, including area check dams and hillside terracing, have

https://doi.org/10.5194/egusphere-2026-3534
Preprint. Discussion started: 20 July 2026

progressively restored vegetation in parts of Tigray and northern Amhara, and the effects of these interventions are detectable in satellite-derived vegetation trends (Descheemaeker et al., 2022; Tesfaye et al., 2017).

The Tekeze Basin has experienced several catastrophic drought events during the study period, including the 2002–2003, 2008–2009, 2015–2016 (El Niño-driven), and 2021–2023 (compounded Tigray conflict–drought) crises, making it a priority region for long-term drought monitoring and early warning system development.

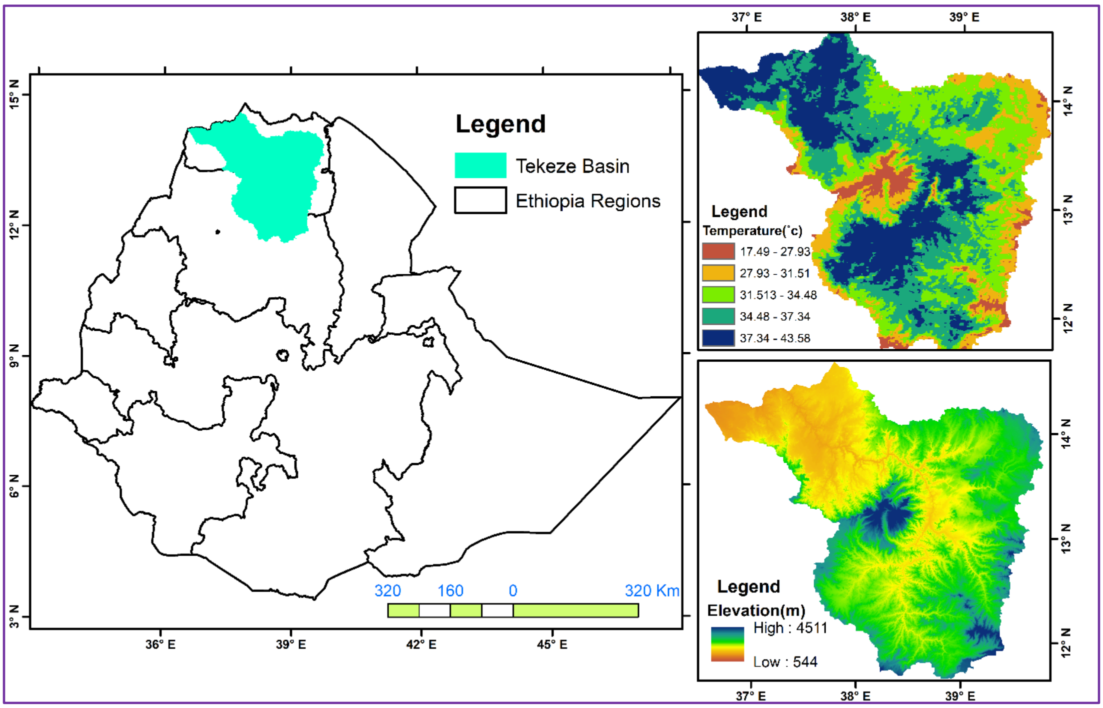

Figure 1. Location map of the Tekeze Basin in Ethiopia, showing its geographical location, major elevation, temperature, and administrative boundaries.

2.2 Datasets

2.2.1 MODIS Vegetation Indices (MOD13Q1 V6.1): The Moderate Resolution Imaging Spectroradiometer (MODIS)/Terra MOD13Q1 product provides NDVI and EVI. NDVI was used to compute VCI, VHI, and NDWI, and to parameterize the dry edge of the TVDI, LST/NDVI feature space (Didan, 2015).

2.2.2 MODIS Land Surface Temperature (MOD11A2 V6.1): The MODIS/Terra MOD11A2 product provides daytime land surface temperature (LST). LST data were used to compute TCI, VHI, and TVDI (Wan et al., 2015).

2.2.3 NASA-USDA SMAP Enhanced L3 Soil Moisture: Surface soil moisture data were obtained from the NASA-USDA Global Soil Moisture product derived from the Soil Moisture Active Passive (SMAP) Level-3 Enhanced passive microwave sensor. SMAP data (available continuously from

https://doi.org/10.5194/egusphere-2026-3534
Preprint. Discussion started: 20 July 2026

April 2015) were supplemented for the 2000–2015 period using the SMAP-Sentinel fusion product and cross-validated with MODIS-based surface moisture proxies (TVDI) to ensure temporal consistency across the full 2000–2025 period. SMCI was derived from these harmonized soil moisture data.

2.2.4 CHIRPS v2.0 Precipitation: Monthly precipitation data from the Climate Hazards Group Infrared Precipitation with Station (CHIRPS) were used to compute PCI. CHIRPS provides quasi-global (~50°N–50°S) daily and monthly precipitation from 1981 to near-present, blending cold cloud duration satellite estimates with in-situ gauge observations. CHIRPS has been rigorously validated over Ethiopia and East Africa and has demonstrated superior performance relative to other gridded products in the region (Funk et al., 2015; Dinku et al., 2018; Ayehu et al., 2018).

2.3 Drought Assessment Methodology

This study integrates four primary remote sensing and climate datasets into a unified Google Earth Engine (GEE) processing platform using Python API in Google Colaboratory. We acquire MODIS MOD13Q1 (version 6) vegetation indices (NDVI, NDWI) at 250 m resolution (16-day composites), MODIS MOD11A2 (version 6) land surface temperature LST) at 1 km resolution (8-day composites), NASA-USDA SMAP enhanced soil moisture at ~9 km resolution, and CHIRPS (version 2) precipitation at ~5.5 km resolution. Within GEE, we compute seven complementary drought indices: the VCI and TCI, which we combine into the VHI; the TVDI derived from the LST-NDVI feature space; the SMCI from SMAP data; PCI from CHIRPS; and NDWI from MODIS reflectance bands. All indices are computed monthly for the six-month growing season (April–September) across the 26-year study period (2000–2025) at 250 m pixel resolution, enabling spatially continuous, temporally consistent characterization of multiple drought dimensions simultaneously. All datasets were reprojected to the WGS84/Geographic coordinate system, and clipped to the Tekeze Basin boundary derived from the HydroSHEDS Level 5 hydrographic dataset (Lehner et al., 2008). These operations were performed within GEE and QGIS. Following index computation in GEE, we apply pixel-wise Mann-Kendall trend testing and Sen's slope estimation to quantify long-term spatiotemporal drought trends across the entire basin, generating trend maps that show both the direction (MK Tau) and magnitude (Sen's slope) of change for each index. In parallel, we use R statistical software (ggplot2, corrplot, and trend packages) to generate multi-year time series graphs showing seasonal dynamics and to compute monthly Pearson correlation matrices revealing inter-index relationships stratified by growing-season month (Wei and Simko, 2017). We then use QGIS for cartographic visualization and composition of publication-quality multi-panel trend maps showing spatial patterns of drought change. This integrated framework yields actionable findings regarding spatiotemporal drought patterns, long-term trends by region and season, and inter-index correlations that directly inform drought early warning system design and climate-smart resource management decisions.

2.4 Drought Indices Extraction

2.4.1 VCI

VCI, developed by Kogan (1990, 1995), quantifies vegetation stress relative to historical NDVI extremes for each pixel and calendar period:

$$VCI=\frac{NDVIt\text{-}NDVImin}{NDVImax\text{-}NDVI\ min}*100\ldots\ldots(1)$$

https://doi.org/10.5194/egusphere-2026-3534
Preprint. Discussion started: 20 July 2026

where $NDVI_{min}$ and $NDVI_{max}$ are the long-term pixel-wise minimum and maximum NDVI computed across 2000–2025. VCI ranges from 0 (extreme drought stress) to 100 (optimal vegetation condition); values below 40 indicate drought (Kogan, 1995; Rhee et al., 2010).

2.4.2 TCI

TCI quantifies thermal stress relative to historical LST extremes:

$$TCI=\frac{LST_{max}-LST_t}{LST_{max}-LST_{min}}*100 \quad (2)$$

where LST_{max} and LST_{min} are pixel-wise long-term extremes. Higher TCI values indicate cooler and more favorable thermal conditions; lower values indicate heat stress associated with drought (Kogan, 1995).

2.4.3 VHI

VHI integrates VCI and TCI into a composite drought severity metric (Kogan, 1997):

$$VHI = \alpha \times VCI + (1 - \alpha) \times TCI \quad (3)$$

where α = 0.5, assigning equal weight to vegetation and thermal components as recommended by Kogan (1997) in the absence of site-specific calibration data. VHI values below 40 indicate drought conditions of varying severity.

2.4.4 TVDI

TVDI was computed following Sandholt et al. (2002) using the LST and NDVI triangle space:

$$TVDI = \frac{LST - LST\_min(NDVI)}{LSTdry(NDVI) - LSTmin(NDVI)} \quad (4)$$

where LST_{min} (NDVI) represents the wet edge (minimum LST for a given NDVI) and LST_{dry} (NDVI) = a + b×NDVI is the dry edge, derived by fitting a linear regression to the upper boundary of the monthly LST/NDVI scatter plot within the basin for each time step. TVDI ranges from 0 (fully wet, no water stress) to 1 (extreme dryness), with higher values indicating greater surface moisture stress (Sandholt et al., 2002; Wang et al., 2004; Holzman et al., 2014).

2.4.5 SMCI

SMCI was derived from SMAP-based soil moisture data following Du et al. (2013):

$$SMCI = \frac{SM - SMmin}{SMmax - SMmin} \quad (5)$$

where SM is observed monthly soil moisture, and SM_{min} and SM_{max} are pixel-wise long-term minima and maxima. SMCI values near 100 indicate wet soil conditions, and values near 0 indicate severe soil moisture drought.

2.4.6 PCI

https://doi.org/10.5194/egusphere-2026-3534
Preprint. Discussion started: 20 July 2026

PCI captures meteorological drought and was computed from CHIRPS monthly precipitation following Rhee et al. (2010):

$$\mathrm{PCI} = \frac{(P-P_{min})}{(P_{max}-P_{max})} * 100 \text{..(6)}$$

where P is the monthly CHIRPS precipitation, and P_{min} and P_{max} are pixel-wise long-term extremes over 2000–2025.

2.4.7 NDWI

NDWI was computed from MODIS surface reflectance bands following Gao (1996):

$$\mathrm{NDWI} = \frac{(\mathrm{Band_{NIR}}-\mathrm{Band_{SWIR}})}{(\mathrm{Band_{NIR}}+\mathrm{Band_{SWIR}})} \text{...(7)}$$

NDWI is sensitive to vegetation liquid water content and soil surface moisture. Values typically range from −1 to +1, with higher values indicating greater moisture availability.

2.5 Mann-Kendall Trend Analysis and Sen's Slope Estimation

Monotonic temporal trends in each drought index time series were assessed pixel-by-pixel using the non-parametric MK test (Mann, 1945; Kendall, 1975). The MK test is widely preferred in hydro-climatic trend analysis due to its robustness to non-normality, seasonality, outliers, and missing data (Hamed and Rao, 1998; Yue and Wang, 2002). The MK statistic S is defined as:

$$S = \sum_{k=1}^{n-1} \sum_{j=k+1}^{n} \mathrm{sgn}\left(x_j - x_k\right) \text{.....................................(8)}$$

where x_k and x_j are data values at time steps k and j, and sgn(·) is the sign function returning +1, 0, or −1. Positive (negative) S indicates an upward (downward) trend. Statistical significance was assessed at the 95% confidence level ($p < 0.05$) using the standardized test statistic Z. The normalized Kendall Tau (τ) was computed as:

$$\tau = S \,/\, (n(n-1)/2) \text{..(9)}$$

and mapped spatially for each index as an indicator of trend direction and relative magnitude. The magnitude of each detected trend was quantified using Sen’s slope estimator (Sen, 1968):

$$\beta = \mathrm{median}\left(\left(x_j - x_k\right)/(j-k)\right) \text{.....................................(10)}$$

Sen’s slope (expressed in index units per year) represents a robust, outlier-resistant estimate of the trend magnitude and was mapped spatially alongside MK Tau to provide both directional and quantitative information about long-term drought change.

2.6 Inter-Index Pearson Correlation Analysis

Monthly Pearson correlation coefficients I were computed between all pairwise combinations of the seven drought indices using a 26-year time series (2000–2025) of basin-averaged monthly mean values. Correlations were considered statistically significant at $p < 0.05$ based on t-tests applied within each monthly matrix.

$$r = \frac{\sum\left((x_i - \bar{x})(y_i - \bar{y})\right)}{\sqrt{\sum(x_i - \bar{x})^2 \sum(y_i - \bar{y})^2}} \text{...(11)}$$

https://doi.org/10.5194/egusphere-2026-3534
Preprint. Discussion started: 20 July 2026

where r is the correlation coefficient, x_i and y_i are paired values, $\bar{x}$ and $\bar{y}$ are the mean values of paired drought indices, respectively.

3. Results

3.1 Temporal Dynamics of Drought Indices (2000–2025)

3.1.2 TCI

TCI time series showed broadly similar seasonal patterns to VCI, with July and August recording the highest values (65–80) and April the lowest (10–25), as shown in Figure 2a. However, TCI exhibited lower interannual variability than VCI in most months, suggesting that land surface temperatures in the Tekeze Basin are less year-to-year variable than vegetation greenness, likely because LST is smoothed by thermal inertia and is not solely controlled by rainfall. A notable feature is the visible upward tendency in July and August TCI from approximately 2018 onward, consistent with the spatially dominant positive trend (82.2% positive coverage) identified in the Mann-Kendall analysis.

3.1.1 VCI

Basin-averaged VCI time series (2000–2025) revealed pronounced seasonal stratification across the six growing-season months (Figure 2b). July and August consistently recorded the highest VCI values (60–85), corresponding to peak Kiremt monsoon activity and maximum greenness, while April and May exhibited the lowest values (10–20), frequently falling below the drought threshold of 40 and indicating moderate to severe vegetation stress during the early growing season. Interannual variability was highest in June (the Kiremt onset month), reflecting the sensitivity of vegetation greenness to the timing and intensity of seasonal rains. Exceptional drought years with basin-wide VCI minima below 15 across all months include 2002–2003, 2008–2009, and 2015–2016, corresponding to documented El Niño events and positive Indian Ocean Dipole (IOD) phases. VCI values showed a gradual increasing tendency in July and August from approximately 2015 onward, consistent with the predominantly positive long-term trend found in the spatial analysis.

3.1.3 VHI

VHI, as the composite of VCI and TCI, closely mirrored VCI temporal patterns across all months (Figure 2c). April values were consistently below 25 across almost all years, representing the most severe composite drought stress period of the growing season. Major drought years (2002–2003, 2009, 2015–2016) were clearly identifiable as multi-month episodes with VHI below 30 across April–June. The August time series showed a modest positive trend since approximately 2012, consistent with the watershed rehabilitation and land restoration programs implemented in Tigray during the 2000s and 2010s.

3.1.4 TVDI

TVDI exhibited an inverse seasonal pattern relative to the vegetation indices (Figure 2d). April and May recorded the highest TVDI values (0.75–0.85), reflecting maximum land surface dryness at the onset of the growing season before Kiremt rains have recharged soil moisture. TVDI decreased progressively from June onward, reaching minima of 0.18–0.28 in July and August at peak canopy

https://doi.org/10.5194/egusphere-2026-3534
Preprint. Discussion started: 20 July 2026

cover and soil moisture. The year 2009 stood out as an extreme year with elevated TVDI across all months. There was no clear basin-mean directional trend in TVDI, although the pixel-wise spatial analysis revealed a dominant basin-wide drying trend (Section 3.2).

Figure 2. Annual time series (2000–2025) of basin-averaged monthly mean values for four drought indices in the Tekeze Basin, Ethiopia, across the growing season months April (pink), May (olive), June (green), July (teal), August (blue), and September (magenta). (a) VCI; 0–100 scale; threshold of 40 denotes drought onset, (b) TCI; 0–100 scale, (c) VHI; composite of VCI and TCI; 0–100 scale, and (d) TVDI; 0–1 scale; higher values indicate greater land surface dryness.

3.1.5 SMCI

SMCI displayed the most extreme seasonal amplitude of all seven indices, with August values consistently reaching 80–95 (near-optimal soil moisture) and April values falling to 5–25 (severe soil moisture drought), reflecting the strongly unimodal rainfall regime of the Tekeze Basin (Figure

https://doi.org/10.5194/egusphere-2026-3534
Preprint. Discussion started: 20 July 2026

3a). Interannual variability was highest in June and September, the Kiremt onset and cessation months, when shifts in the rainy season timing translate directly into large differences in soil water availability. The April SMCI time series showed a modest but visible declining tendency post-2015, consistent with negative SMCI trends detected in the spatial analysis and potentially indicating a progressive deepening of early growing-season moisture deficits.

3.1.6 PCI

PCI exhibited the highest interannual variability of all indices, particularly in April and May where the coefficient of variation exceeded 45% in most years (Figure 3b). July and August recorded the highest PCI values in wet years (70–100), while April PCI frequently approached 0 across dry years, indicating near-complete absence of rainfall relative to the long-term maximum. Major drought years were clearly identifiable as multi-month PCI minima: 2002–2003, 2008–2009, and 2015–2016.

3.1.7 NDWI

NDWI values remained consistently low throughout the study period (−0.05 to +0.16), reflecting the dominantly semi-arid land surface character of the basin (Figure 3c). A visible positive trend emerged across all months from approximately 2010 onward, with the most pronounced increases in August and September post-2020. This positive NDWI trajectory is the strongest long-term directional signal visible in the basin-mean time series and aligns closely with the spatial trend analysis showing 86.4% positive NDWI coverage across the basin.

https://doi.org/10.5194/egusphere-2026-3534
Preprint. Discussion started: 20 July 2026

Figure 3. Annual time series (2000–2025) of basin-averaged monthly mean values for three additional drought indices in the Tekeze Basin, Ethiopia, across growing season months (color coding as in Figure 2). (a) SMCI; 0–100 scale, (b) PCI; 0–100 scale, (c) NDWI; −1 to +1 scale.

3.2 Spatiotemporal Drought Trend Maps

3.2.1 VCI, TCI, and VHI Trends

The spatial distribution of MK Tau (Figure 4a) and Sen's slope (Figure 4b) for VCI revealed predominantly positive trends across 71.5% of the basin area. Positive MK Tau values (indicating improving vegetation condition) were most pronounced in the central and southeastern portions of the basin at mid-elevations, with Tau values reaching up to +0.636. Negative trends (Tau as low as −0.557) were concentrated in the northern sub-basin, particularly in the Tigray highlands near the Eritrean border and in isolated pockets in the western lowland margins. Sen's slope for VCI ranged from −0.006 to +0.008 VCI units per year. TCI showed even more dominant positive trends, with 82.2% positive coverage and Tau ranging from −0.447 to +0.573(Figure 4c), while Sen's slope (Figure 4d) spanned −0.003 to +0.004 TCI units per year. VHI spatial trends closely mirrored VCI and TCI combined patterns, with 74.8% positive coverage and MK Tau (Figure 4e) ranging from −0.470 to +0.605, and Sen's slope (Figure 4f) from −0.004 to +0.006 VHI units per year. The spatial coherence between VCI, TCI, and VHI trend patterns indicates expected internal consistency of the multi-index dataset.

https://doi.org/10.5194/egusphere-2026-3534
Preprint. Discussion started: 20 July 2026

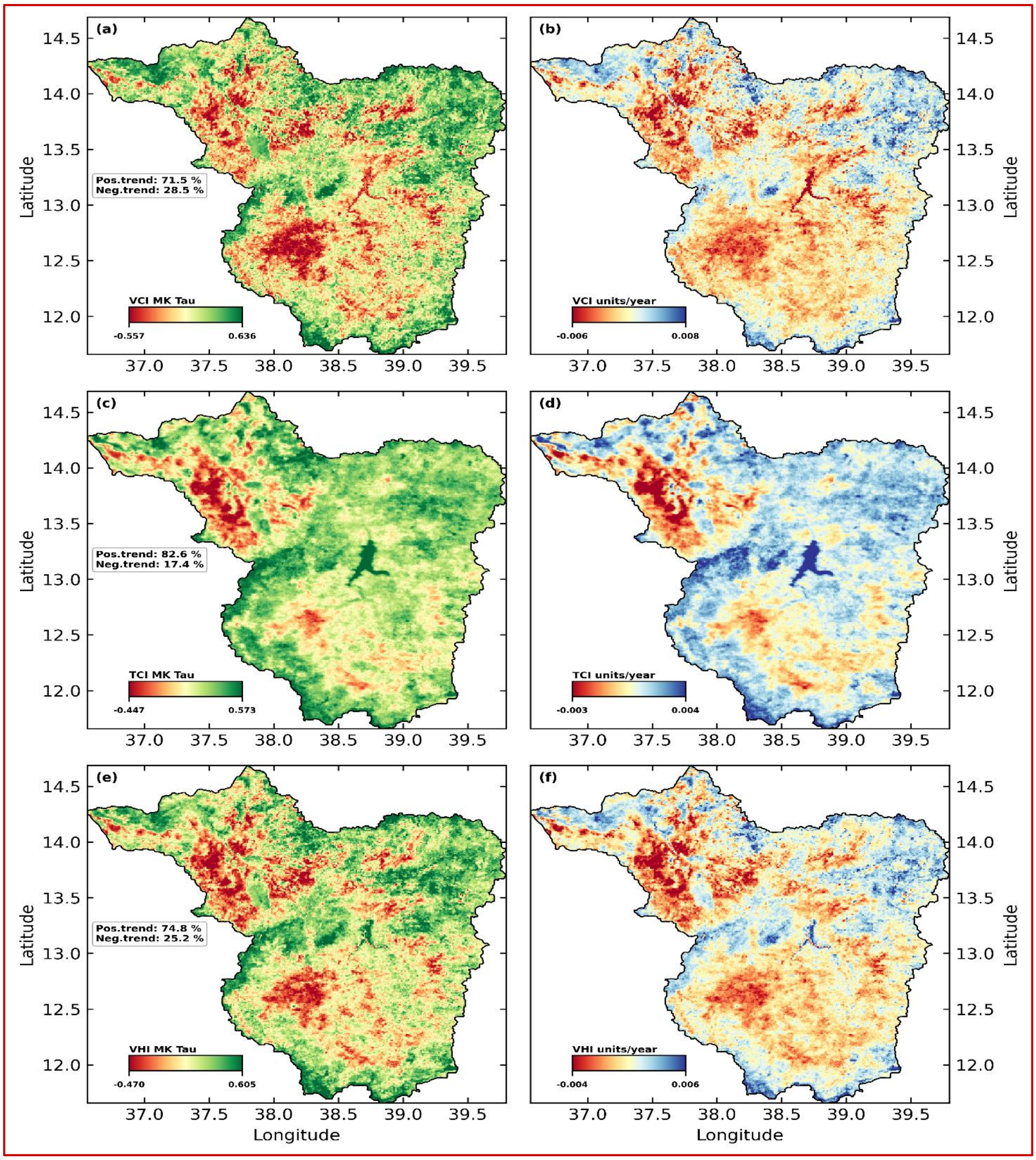

Figure 4. Spatial distribution of Mann-Kendall Tau (τ; left column) and Sen's slope in units per year (right column) for three vegetation-based drought indices in the Tekeze Basin, computed from 2000–2025 monthly growing-season time series. (a) VCI: MK Tau, (b) VCI: Sen's slope, (c) TCI: MK Tau, (d) TCI: Sen's slope, (e) VHI: MK Tau, and (f) VHI: Sen's slope. Green tones in MK Tau maps indicate improving (less drought) trends; red tones indicate deteriorating (more drought) trends. Blue tones in Sen's slope maps indicate positive (improving) change; red-orange tones indicate negative (worsening) change. Black outline denotes the Tekeze Basin boundary.

https://doi.org/10.5194/egusphere-2026-3534
Preprint. Discussion started: 20 July 2026

3.2.2 PCI Trends

PCI exhibited the most spatially heterogeneous trend pattern of all indices, with 54.7% negative trend coverage predominantly in the northern and northeastern sub-basins. MK Tau (Figure 5g) ranged from −0.304 to +0.360, and Sen's slope (Figure 5h) from −0.019 to +0.022 PCI units per year. The positive PCI Sen's slope reached the highest magnitude of any index (+0.022), reflecting large absolute interannual variability in precipitation.

3.2.3 TVDI Trends

TVDI exhibited a strikingly different trend pattern from the vegetation indices: 82.2% of the basin area showed negative MK Tau values, indicating increasing land surface dryness (higher TVDI) over the study period. This represents the strongest and most spatially consistent negative trend signal detected across all seven indices. MK Tau (Figure 5i) ranged from −0.613 to +0.375, with the most negative values concentrated in the basin interior and the Afar lowlands. Positive TVDI trends (wetting tendencies) were confined to limited areas in the northwestern highlands. Sen's slope (Figure 5j) ranged from −0.005 to +0.002 TVDI units per year. This finding that land surface dryness is increasing while vegetation condition is improving reveals an important decoupling between above-ground greenness and surface energy balance dryness that has significant implications for drought assessment (see Section 5.1).

3.2.4 SMCI Trends

SMCI showed 55.3% negative trend coverage, indicating that soil moisture conditions have deteriorated across more than half the basin. The strongest negative SMCI trends (MK Tau as low as −0.929, the most negative of all indices in this study) were found in the central basin and the eastern lowlands (Figure 5k). The extremely wide Sen's slope (Figure 5l) range (−0.145 to +0.135 SMCI units per year) reflects high spatial variability in soil moisture trend trajectories, driven by topographic and land-cover gradients. Positive SMCI trends were observed in portions of the northwestern highlands and along the Tekeze main river corridor, potentially reflecting reservoir effects and rehabilitation-induced surface hydrological changes.

https://doi.org/10.5194/egusphere-2026-3534
Preprint. Discussion started: 20 July 2026

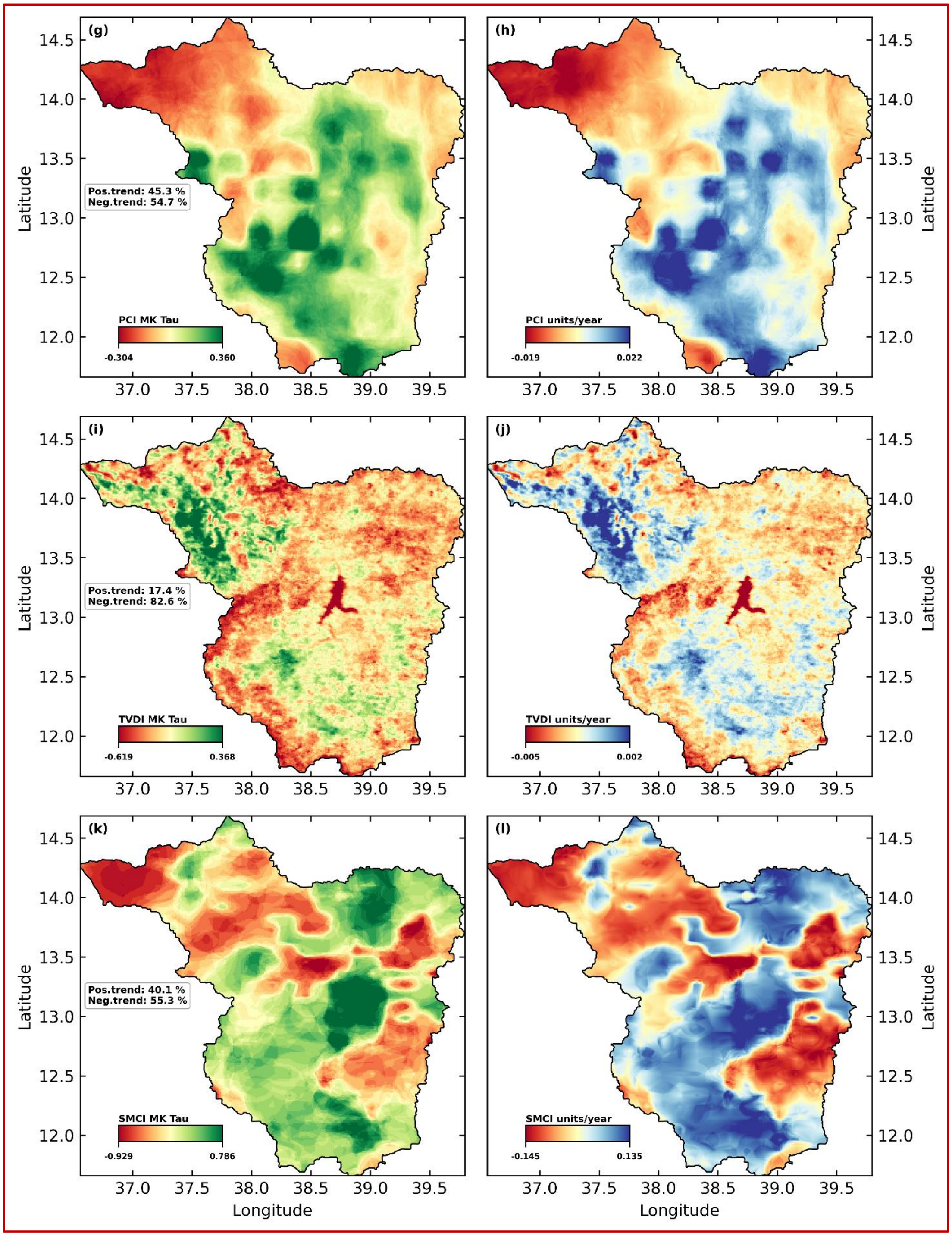

https://doi.org/10.5194/egusphere-2026-3534
Preprint. Discussion started: 20 July 2026

Figure 5. Spatial distribution of Mann-Kendall Tau (τ; left column) and Sen's slope in units per year (right column) for three additional drought indices in the Tekeze Basin. (g) PCI: MK Tau, (h) PCI: Sen's slope, (i) TVDI: MK Tau, (j) TVDI: Sen's slope, (k) SMCI: MK Tau, and (l) SMCI: Sen's slope. Note: Green tones in MK Tau maps indicate improving (less drought) trends; red tones indicate deteriorating (more drought) trends. Blue tones in Sen's slope maps indicate positive (improving) change; red-orange tones indicate negative (worsening) change. Black outline denotes the Tekeze Basin boundary.

3.2.5 NDWI Trends

NDWI showed the highest proportion of positive trends of all seven indices, with 86.4% positive MK Tau coverage across the basin. MK Tau (Figure 6m) ranged from −0.455 to +0.723, and Sen's slope (Figure 6n) from −0.005 to +0.003 NDWI units per year. The small negative Sen's slope pockets were confined to the northern sub-basin, consistent with negative VCI and PCI trends in the same area.

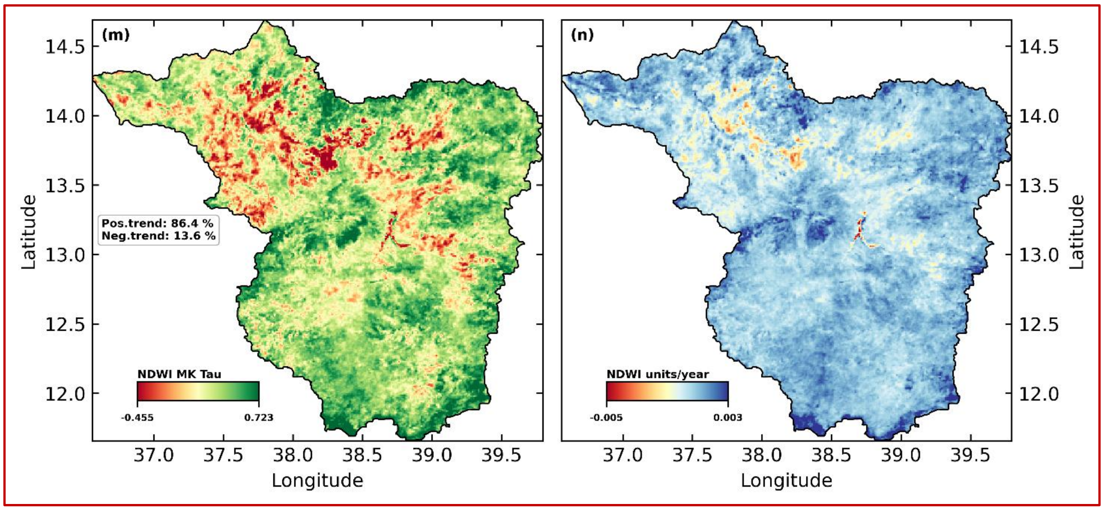

Figure 6. Spatial distribution of Mann-Kendall Tau (τ; left column) and Sen's slope in units per year (right column) for four additional drought indices in the Tekeze Basin. (m) NDWI: MK Tau, (n) NDWI: Sen's slope. Note: Green tones in MK Tau maps indicate improving (less drought) trends; red tones indicate deteriorating (more drought) trends. Blue tones in Sen's slope maps indicate positive (improving) change; red-orange tones indicate negative (worsening) change. Black outline denotes the Tekeze Basin boundary.

3.3 Monthly Inter-Index Correlation Analysis

3.3.1 Overall Correlation Structure

Monthly Pearson correlation analysis (Figure 7) revealed consistent and physically interpretable inter-index relationships across all six growing-season months. The most robust positive relationship was between TCI and VCI (r = 0.48 to 0.97 across months), confirming the tight mechanistic coupling between thermal stress reduction and vegetation greenness improvement, both driven primarily by soil moisture availability. The strongest negative relationships were between TVDI and VHI (r = −0.54 to −0.97), and between TVDI and VCI (r = −0.48 to −0.92), which is an inverse relationship between land surface dryness and vegetation health.

https://doi.org/10.5194/egusphere-2026-3534
Preprint. Discussion started: 20 July 2026

3.3.2 April Correlations

In April, the earliest and most drought-stressed month, TCI–VCI correlation was moderate (r = 0.48) and TVDI and VHI were strongly negative (r = −0.97). The extreme TVDI and VHI coupling in April reflects the dominance of thermal-moisture stress in controlling composite vegetation health during the late dry season, before the Belg rains have significantly recharged soil water. PCI showed the weakest correlations with other indices in April (r = 0.19–0.35), consistent with the short lag between rainfall onset and vegetation or soil moisture response.

3.3.3 May and June Correlations

From May to June, as the Belg rains progress and soils begin to wet up, PCI and SMCI correlations strengthened substantially (from r = 0.19 in April to r = 0.72 in June), indicating that precipitation is increasingly translating into measurable soil moisture recharge by June. The VCI and PCI correlation reached r = 0.82 in June. TVDI and VHI and TVDI and VCI relationships remained strongly negative through June (r = −0.86 and −0.84 in June, respectively), and TCI and VCI strengthened to r = 0.86.

3.3.4 July and August Correlations

July and August yielded the strongest overall inter-index correlations, consistent with peak Kiremt monsoon activity and maximum seasonal moisture differentiation between wet and dry years. TCI and VCI correlation in July reached r = 0.55–0.82, and VCI and VHI reached r = 0.92. The SMCI–PCI correlation was 0.73 in July and 0.57 in August, reflecting the time-integrated effect of cumulative rainfall on soil water stores. TVDI and VHI weakened slightly to r = −0.63 in August relative to its April peak of −0.97, suggesting that the relative influence of thermal stress on composite vegetation health diminishes when water availability is at its seasonal maximum.

3.3.5 September Correlations

In September, the Kiremt cessation month, VCI and VHI correlations remained very strong (r = 0.96), and TCI and VCI was 0.84, indicating continued tight biophysical coherence during the late rainy season. PCI–SMCI correlation was 0.54, and NDWI and SMCI was 0.42, consistent with soil water stores still being replenished by residual rains and reflected in both canopy water content (NDWI) and root-zone moisture (SMCI). PCI and TVDI showed its strongest negative correlation in September (r = −0.54), confirming that precipitation is a primary control on land surface dryness during the late growing season.

https://doi.org/10.5194/egusphere-2026-3534
Preprint. Discussion started: 20 July 2026

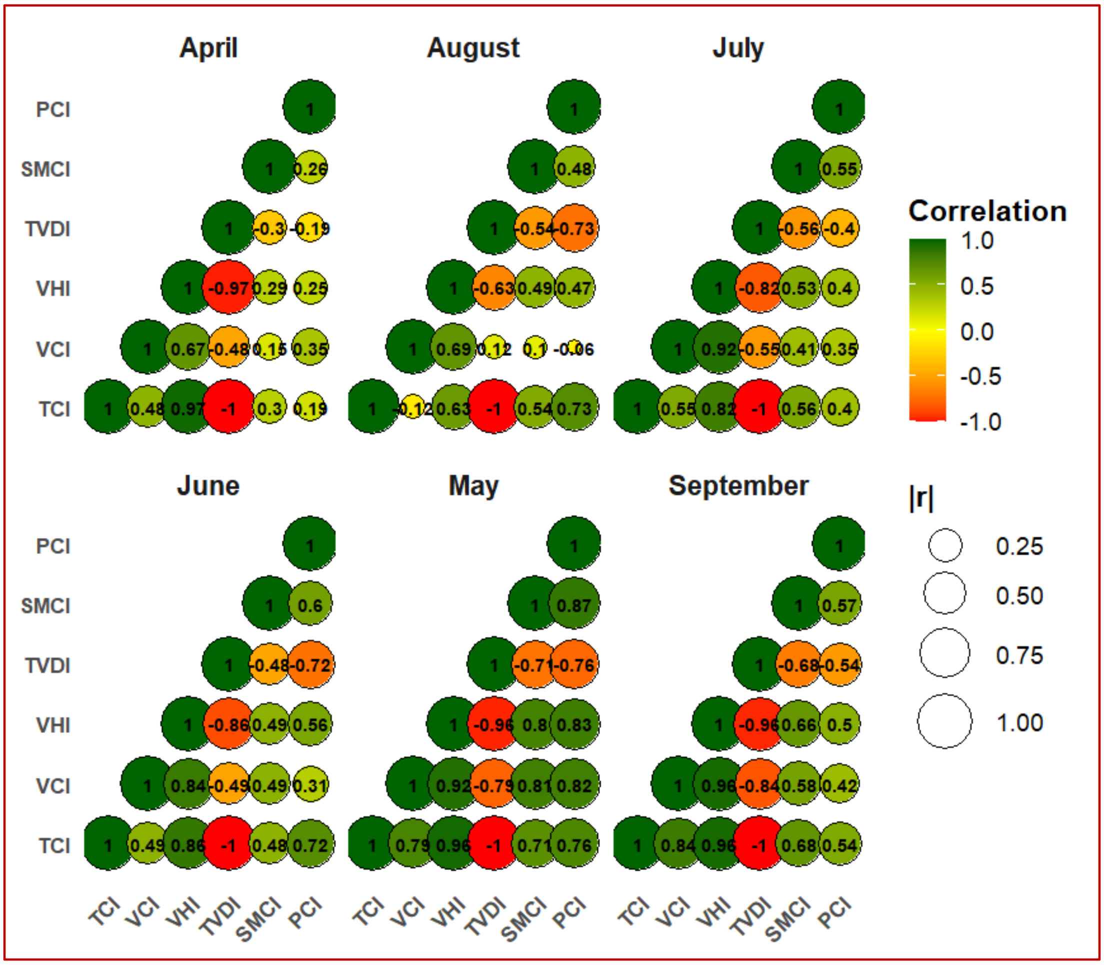

Figure 7. Monthly Pearson correlation matrices (corrplots) for all pairwise combinations of seven drought indices (VCI, TCI, VHI, TVDI, SMCI, PCI) in the Tekeze Basin, computed from 26-year (2000–2025) basin-averaged monthly time series. Results are shown for six growing-season months: April, May, June, July, August, and September. Circle color indicates the direction and magnitude of correlation: dark green = strong positive correlation (r approaching +1.0); red/orange = strong negative correlation (r approaching −1.0); intermediate colors indicate weaker correlations. Circle size is proportional to the absolute correlation coefficient |r|. All correlations with $p < 0.05$ (two-tailed t-test) are shown; non-significant correlations would appear smaller.

4. Discussion

5.1 Complementarity of Multi-Index Drought Assessment

A fundamental finding of this study is that the seven drought indices capture distinct and only partially overlapping dimensions of drought in the Tekeze Basin, validating the necessity of multi-index frameworks argued by AghaKouchak et al. (2015), Wilhite et al. (2014), and Yao et al. (2020).

https://doi.org/10.5194/egusphere-2026-3534
Preprint. Discussion started: 20 July 2026

The most striking divergence is between positive trends in vegetation-based indices (VCI, TCI, VHI, NDWI) and negative trends in soil moisture and land surface dryness indices (TVDI, SMCI). This apparent paradox vegetation improving while soil moisture and surface dryness worsen has been increasingly documented in dryland systems globally and has been attributed to: (1) CO_2 fertilization, which enables vegetation to maintain canopy greenness at reduced soil moisture through improved intrinsic water use efficiency (Liu et al., 2020); (2) species-level compositional shifts toward drought-tolerant vegetation types that maintain greenness under drier conditions; (3) the disproportionate statistical influence of a few extreme wet years on VCI/NDWI long-term means, while median soil moisture conditions deteriorate; and (4) the selective response of above-ground greenness to watershed rehabilitation programs, which may increase leaf area index without proportionally restoring soil water-holding capacity or surface energy balance (Descheemaeker et al., 2022; Brandt et al., 2017). These mechanisms are not mutually exclusive and are likely acting in concert across the Tekeze Basin. The lesson for drought monitoring practitioners is clear: an assessment based solely on VCI or VHI would generate an optimistic but potentially misleading characterization of drought trends in this basin, while exclusive reliance on TVDI or SMCI would overstate deterioration. Only a multi-index framework reveals the full complexity.

4.2 Spatial Heterogeneity and Sub-Basin Vulnerability

The spatial trend maps expose marked within-basin heterogeneity that would be entirely invisible in station-based or catchment-averaged drought assessments. The northern Tekeze sub-basin, particularly the Tigray highlands and the Eritrean border zone, consistently emerged as the most drought-vulnerable area, exhibiting negative trends simultaneously in VCI, VHI, and PCI. This spatial convergence of degrading trends across multiple indices strongly suggests a persistent and worsening drought hotspot in the northern basin, consistent with documented declines in Kiremt season rainfall in northern Ethiopia reported by Seleshi and Zanke (2004), Conway et al. (2009), Gebremeskel et al. (2019), and Haile et al. (2020), and likely exacerbated by the 2020–2022 Tigray conflict, which disrupted land management and rehabilitation activities. In contrast, the central basin showed predominantly positive multi-index trends, potentially reflecting the positive hydrological and vegetation effects of the Tekeze Hydropower Reservoir (post-2009), ongoing watershed exclosure programs, and elevation-dependent rainfall redistribution.

4.3 Seasonal Dynamics and Growing Season Implications

The temporal analysis consistently identified April and May as the most drought-stressed months across all indices, with VCI, TCI, VHI, SMCI, PCI, and NDWI at or near their seasonal minima and TVDI at its seasonal maximum during this pre-monsoon period. This finding has direct implications for agricultural planning: smallholder farmers in the Tekeze Basin who plant rain-fed crops in March to April are exposed to the highest drought risk at the planting and early establishment stage, before Kiremt rains materialize. Integrating PCI and SMCI into drought early warning during March–May when these indices can detect emerging moisture deficits weeks before vegetation stress becomes visible in NDVI-based products would provide a critical 2–4 week lead time advantage for timely agricultural interventions and livelihood protection decisions (Rhee et al., 2010; AghaKouchak et al., 2015).

4.4 Inter-Index Relationships and Physical Mechanisms

https://doi.org/10.5194/egusphere-2026-3534
Preprint. Discussion started: 20 July 2026

The strong and consistent TCI and VCI positive correlations (up to r = 0.97 in April) confirm the tight thermal-vegetation coupling in this semi-arid system: as soil moisture increases with advancing rains, both canopy transpiration (cooling LST, raising TCI) and vegetation greenness (raising NDVI, raising VCI) respond simultaneously (Sandholt et al., 2002; Wang et al., 2004). The strong TVDI and VHI negative relationship (up to r = −0.97 in April and May) demonstrates that TVDI is a reliable inverse proxy for composite vegetation health in this basin. The progressive strengthening of PCI–SMCI correlations from April (r ≈ 0.19) to June (r ≈ 0.72) reveals the seasonal buildup of the precipitation–soil moisture linkage as cumulative Kiremt rains progressively fill soil water stores. The relatively weaker PCI and TVDI negative correlations compared to SMCI and TVDI across all months confirm that TVDI responds primarily to the integrated soil moisture state rather than instantaneous precipitation events, a distinction important for designing multi-index early warning systems (Du et al., 2013).

4.5 Methodological Contributions

This study makes a methodological contribution by demonstrating the effective integration of Google Earth Engine Python Colab for large-scale pixel-wise trend computations, R software for rigorous statistical analysis and visualization, and QGIS for publication-quality cartographic outputs a combined workflow that is reproducible, open-source, and transferable to other data-scarce basins across Africa. The GEE Python Colab environment proved particularly powerful for pixel-wise MK and Sen's slope computation across 82,000 km² at 250 m resolution without requiring local computational infrastructure, enabling a level of spatial detail and temporal scope not achievable with traditional local-computing workflows. This framework is fully extensible to additional drought indices, additional basins, and future climate projections.

4.6 Limitations and Future Research Directions

Several limitations of this study should be acknowledged. First, SMAP soil moisture data are available only from April 2015 at standard quality, requiring gap-filling or surrogate estimation for 2000–2015 SMCI computation, which may introduce uncertainty into early-period trend estimates. Second, MODIS 16-day composites cannot fully capture sub-monthly drought onset dynamics, potentially missing the full intensity of short-duration drought events. Third, the pixel-wise MK trend analysis does not correct for spatial autocorrelation between adjacent pixels, which may inflate the effective degrees of freedom and affect the interpretation of statistical significance thresholds. Fourth, the analysis does not include a formal quantitative attribution of detected trends to climate variability versus land use change versus land rehabilitation interventions, a direction that warrants future investigation using multivariate attribution frameworks. Future studies should: (1) integrate ground-based soil moisture, streamflow, and agricultural yield data for multi-source validation of the remote sensing indices; (2) investigate the role of large-scale climate drivers (ENSO, IOD, AMO) in modulating interannual drought variability across the basin; (3) extend the multi-index framework to include projected future drought changes using CMIP6 regional climate model outputs; and (4) develop a composite drought vulnerability index for the Tekeze Basin integrating the seven indices and socioeconomic exposure data for targeted policy applications.

https://doi.org/10.5194/egusphere-2026-3534
Preprint. Discussion started: 20 July 2026

5. Conclusions

This study delivered the first comprehensive multi-index, pixel-scale spatiotemporal drought analysis in the Tekeze Basin, Ethiopia, integrating seven satellite-derived drought indices (VCI, TCI, VHI, TVDI, SMCI, PCI, NDWI) computed from MODIS, SMAP, and CHIRPS datasets across the full growing season (April to September) for the period 2000–2025. Index computation and trend analysis were performed in Google Earth Engine Python Colab; statistical charts and correlation matrices were produced in R; and spatial visualization was conducted in QGIS. The principal conclusions are:

(1) Strong seasonal drought gradients: April and May consistently exhibited the most severe drought stress across all indices (VCI ≈ 10–20; SMCI ≈ 5–25; TVDI ≈ 0.75–0.85), while July and August were the most favorable months, highlighting the pre-monsoon period as the highest-risk window for agricultural drought impacts.

(2) Divergence between vegetation and moisture trends: Vegetation-based indices showed predominantly improving trends (VCI: 71.5% positive; TCI: 82.2%; VHI: 74.8%; NDWI: 86.4%), while soil moisture and dryness indices showed dominant negative trends (TVDI: 82.2% negative; SMCI: 55.3%; PCI: 54.7%), revealing a decoupling between above-ground greenness and below-ground moisture status that can only be detected through multi-index analysis.

(3) Persistent northern sub-basin drought hotspot: The northern Tekeze sub-basin (Tigray highlands) showed negative trends simultaneously in VCI, VHI, and PCI, the most severe and multi-dimensionally consistent drought deterioration in the basin, warranting priority attention in drought early warning and resilience investment planning.

(4) Strong biophysical inter-index coupling: TCI and VCI correlations (r up to 0.97) and TVDI and VHI correlations (r down to −0.97) confirmed tight thermal-vegetation linkages across all months, with inter-index correlations strengthening progressively from April to August as the Kiremt monsoon advances. PCI and SMCI linkages strengthened from April ($r \approx 0.19$) to June ($r \approx 0.72$), reflecting the seasonal soil moisture recharge dynamics.

(5) Value of multi-index integration: No single drought index adequately captured all dimensions of drought in the Tekeze Basin. The seven-index framework revealed complementary drought signals undetectable by any individual index and provides a robust foundation for multi-dimensional drought early warning system design in Ethiopia and comparable dryland basins across East Africa.

The open-source, cloud-computing-based multi-index drought monitoring framework developed in this study is transferable to other data-scarce semi-arid basins in sub-Saharan Africa and provides a timely methodological reference for drought researchers and operational agencies engaged in climate-smart natural hazard management.

https://doi.org/10.5194/egusphere-2026-3534
Preprint. Discussion started: 20 July 2026

Data Availability Statement

All input datasets used in this study are publicly accessible: MODIS MOD13Q1 and MOD11A2 products are available via NASA Earthdata (https://earthdata.nasa.gov). NASA-USDA SMAP soil moisture data are available at NASA Earthdata and the GEE data catalog. CHIRPS v2.0 precipitation data are available from the Climate Hazards Center, University of California, Santa Barbara (https://www.chc.ucsb.edu/data/chirps). Analysis scripts (GEE Python Colab notebooks and R code) are available from the corresponding author upon reasonable request.

Author Contributions

(Bedasa Asefa) Conceptualization, methodology, visualization (QGIS), writing original draft, writing review, and editing. (Jianjun Zhao) Conceptualization, methodology, writing, review, and editing, supervision. (*Hongyan Zhang)* Data acquisition and validation, MODIS and CHIRPS dataset processing, quality assurance/quality control, literature review, writing, review, and editing. (*Zhengxiang Zhang*) Study area characterization, interpretation of spatiotemporal patterns, writing, review, and editing. (*Xiaoyi Guo*) Funding acquisition, project administration, institutional support, supervision, writing, review, and editing. (Mebrahtom Zerom) formal analysis, data curation, Google Earth Engine Python scripting, Mann-Kendall trend analysis. (Yosef Ermias) R statistical analysis, correlation matrix computation, temporal graphing, and interpretation of results. (*Andeptop Sule)* hydrological and climatic context, field knowledge of the Tekeze Basin,

Competing Interests

The authors declare that they have no conflict of interest.

Financial Support

This study received no external funding.

Acknowledgements

This work was financially supported by the National Natural Science Foundation of China (Grant Nos. 42471383, 42171321, 42471359), the Science and Technology Development Plan Project of Jilin Province, China (Project No.20260203090SF). The authors gratefully acknowledge NASA, the USGS, and the MODIS science team for providing MODIS MOD13Q1 and MOD11A2 products. The NASA-USDA SMAP team and the Climate Hazards Center (CHIRPS) at the University of California, Santa Barbara are acknowledged for making their datasets publicly available. Google Earth Engine is acknowledged for providing a cloud computing platform used for index computation and trend analysis.

References

AghaKouchak, A., Farahmand, A., Melton, F. S., Teixeira, J., Anderson, M. C., Wardlow, B. D., and Hain, C. R.: Remote sensing of drought: Progress, challenges and opportunities, Rev. Geophys., 53, 452–480, https://doi.org/10.1002/2014RG000456, 2015.

https://doi.org/10.5194/egusphere-2026-3534
Preprint. Discussion started: 20 July 2026

Awange, J. L., Forootan, E., Kuhn, M., Kusche, J., and Heck, B.: Water storage changes and climate variability within the Nile Basin derived from GRACE and climate models, Adv. Water Resour., 73, 1–15, https://doi.org/10.1016/j.advwatres.2014.06.013, 2024.

Ayehu, G. T., Tadesse, T., Gessesse, B., and Dinku, T.: Validation of new satellite rainfall products over the Upper Blue Nile Basin, Ethiopia, Atmos. Meas. Tech., 11, 1921–1936, https://doi.org/10.5194/amt-11-1921-2018, 2018.

Ayana, E. K., Worqlul, A. W., Dile, Y. T., and Srinivasan, R.: Spatiotemporal variability of drought in Ethiopia using remote sensing and rainfall data, Remote Sens., 14, 1982, https://doi.org/10.3390/rs14091982, 2022.

Bewket, W. and Conway, D.: A note on the temporal and spatial variability of rainfall in the drought-prone Amhara region of Ethiopia, Int. J. Climatol., 27, 1467–1477, https://doi.org/10.1002/joc.1481, 2007.

Birara, H., Pandey, R. P., and Mishra, S. K.: Trend and variability analysis of rainfall and temperature in Tikur Wuha watershed, J. Water Clim. Change, 9, 588–596, https://doi.org/10.2166/wcc.2018.041, 2018.

Brandt, M., Rasmussen, K., Peñuelas, J., Tian, F., Schurgers, G., Verger, A., Mertz, O., Palmer, J. R. B., and Fensholt, R.: Human population growth offsets climate-driven increase in woody vegetation in sub-Saharan Africa, Nat. Ecol. Evol., 1, 0081, https://doi.org/10.1038/s41559-017-0081, 2017.

Conway, D., Mould, C., and Bewket, W.: Over one century of rainfall and temperature observations in Addis Ababa: Trends, variability and extremes, Int. J. Climatol., 24, 1981–2002, https://doi.org/10.1002/joc.1134, 2009.

Dai, A.: Increasing drought under global warming in observations and models, Nat. Clim. Change, 3, 52–58, https://doi.org/10.1038/nclimate1633, 2013.

Descheemaeker, K., Nyssen, J., Poesen, J., Raes, D., Haile, M., Muys, B., and Deckers, S.: Runoff on slopes with restoring vegetation: A case study from the Tigray highlands, Ethiopia, J. Hydrol., 331, 219–241, https://doi.org/10.1016/j.jhydrol.2006.05.015, 2022.

Didan, K.: MOD13Q1 MODIS/Terra Vegetation Indices 16-Day L3 Global 250 m SIN Grid V006, NASA EOSDIS Land Processes DAAC, https://doi.org/10.5067/MODIS/MOD13Q1.006, 2015.

Dinku, T., Funk, C., Peterson, P., Maidment, R., Tadesse, T., Gadain, H., and Ceccato, P.: Validation of the CHIRPS satellite rainfall estimates over eastern Africa, Q. J. Roy. Meteorol. Soc., 144, 292–312, https://doi.org/10.1002/qj.3244, 2018.

Diro, G. T., Grimes, D. I. F., and Black, E.: Teleconnections between Ethiopian summer rainfall and sea surface temperature: Part I – Observation and modelling, Clim. Dynam., 37, 103–119, https://doi.org/10.1007/s00382-010-0837-8, 2011.

Du, L., Tian, Q., Yu, T., Meng, Q., Jancso, T., Udvardy, P., and Huang, Y.: A comprehensive drought monitoring method integrating MODIS and TRMM data, Int. J. Appl. Earth Obs. Geoinf., 23, 245–253, https://doi.org/10.1016/j.jag.2012.09.010, 2013.

Funk, C., Peterson, P., Landsfeld, M., Pedreros, D., Verdin, J., Shukla, S., Husak, G., Rowland, J., Harrison, L., Hoell, A., and Michaelsen, J.: The climate hazards infrared precipitation with stations — a new environmental record for monitoring extremes, Sci. Data, 2, 150066, https://doi.org/10.1038/sdata.2015.66, 2015.

Gao, B. C.: NDWI — A normalized difference water index for remote sensing of vegetation liquid water from space, Remote Sens. Environ., 58, 257–266, https://doi.org/10.1016/S0034-4257(96)00067-3, 1996.

Gebre, S. L., Kibru, T., Tesfaye, S., and Taye, G.: Analysis of watershed attributes for water resources management using GIS: The case of Chelekot micro-watershed, Tigray, Ethiopia, J. Geogr. Inf. Syst., 7, 177–190, https://doi.org/10.4236/jgis.2015.72015, 2015.

https://doi.org/10.5194/egusphere-2026-3534
Preprint. Discussion started: 20 July 2026

Gebremeskel, G., Tang, Q., Sun, S., Huang, Z., Zhang, X., and Liu, X.: Droughts in East Africa: Causes, impacts and resilience, Earth-Sci. Rev., 193, 146–161, https://doi.org/10.1016/j.earscirev.2019.04.015, 2019.

Gebremicael, T. G., Mohamed, Y. A., Betrie, G. D., van der Zaag, P., and Teferi, E.: Trend analysis of runoff and sediment fluxes in the Upper Blue Nile basin: A combined analysis of statistical tests, physically-based models and land use maps, J. Hydrol., 482, 57–68, https://doi.org/10.1016/j.jhydrol.2012.12.023, 2013.

Gorelick, N., Hancher, M., Dixon, M., Ilyushchenko, S., Thau, D., and Moore, R.: Google Earth Engine: Planetary-scale geospatial analysis for everyone, Remote Sens. Environ., 202, 18–27, https://doi.org/10.1016/j.rse.2017.06.031, 2017.

Haile, G. G., Tang, Q., Hosseini-Moghari, S. M., Liu, X., Gebremicael, T. G., Leng, G., Kebede, A., Xu, X., and Yun, X.: Projected impacts of climate change on drought patterns over East Africa, Earth's Future, 8, e2020EF001502, https://doi.org/10.1029/2020EF001502, 2020.

Hamed, K. H. and Rao, A. R.: A modified Mann-Kendall trend test for autocorrelated data, J. Hydrol., 204, 182–196, https://doi.org/10.1016/S0022-1694(97)00125-X, 1998.

Holzman, M. E., Rivas, R., and Piccolo, M. C.: Estimating soil moisture and the relationship with crop yield using surface temperature and vegetation index, Int. J. Appl. Earth Obs. Geoinf., 28, 181–192, https://doi.org/10.1016/j.jag.2013.12.006, 2014.

Jiao, W., Wang, L., Smith, W. K., Chang, Q., Wang, H., and D'Odorico, P.: Observed increasing water constraint on vegetation growth over the last three decades, Nat. Commun., 12, 3777, https://doi.org/10.1038/s41467-021-24016-9, 2021.

Kendall, M. G.: Rank Correlation Methods, 4th edn., Charles Griffin, London, 1975.

Kogan, F. N.: Remote sensing of weather impacts on vegetation in non-homogeneous areas, Int. J. Remote Sens., 11, 1405–1419, https://doi.org/10.1080/01431169008955102, 1990.

Kogan, F. N.: Application of vegetation index and brightness temperature for drought detection, Adv. Space Res., 15, 91–100, https://doi.org/10.1016/0273-1177(95)00079-T, 1995.

Kogan, F. N.: Global drought watch from space, Bull. Am. Meteorol. Soc., 78, 621–636, https://doi.org/10.1175/1520-0477(1997)078<0621:GDWFS>2.0.CO;2, 1997.

Lehner, B., Verdin, K., and Jarvis, A.: New global hydrography derived from spaceborne elevation data, Eos Trans. AGU, 89, 93–94, https://doi.org/10.1029/2008EO100001, 2008.

Liu, Y., Kumar, M., Katul, G. G., Feng, X., and Konings, A. G.: Plant hydraulics accentuates the effect of atmospheric moisture stress on transpiration, Nat. Clim. Change, 10, 691–695, https://doi.org/10.1038/s41558-020-0781-5, 2020.

Mann, H. B.: Nonparametric tests against trend, Econometrica, 13, 245–259, https://doi.org/10.2307/1907187, 1945.

Masih, I., Maskey, S., Mussá, F. E. F., and Trambauer, P.: A review of droughts on the African continent: A geospatial and long-term perspective, Hydrol. Earth Syst. Sci., 18, 3635–3649, https://doi.org/10.5194/hess-18-3635-2014, 2014.

McFeeters, S. K.: The use of the Normalized Difference Water Index (NDWI) in the delineation of open water features, Int. J. Remote Sens., 17, 1425–1432, https://doi.org/10.1080/01431169608948714, 1996.

McKee, T. B., Doesken, N. J., and Kleist, J.: The relationship of drought frequency and duration to time scales, Proceedings of the 8th Conference on Applied Climatology, Anaheim, CA, American Meteorological Society, 179–183, 1993.

https://doi.org/10.5194/egusphere-2026-3534
Preprint. Discussion started: 20 July 2026

Nicholson, S. E.: The ITCZ and the seasonal cycle over equatorial Africa, Bull. Am. Meteorol. Soc., 99, 337–348, https://doi.org/10.1175/BAMS-D-16-0287.1, 2018.

Nyssen, J., Poesen, J., Moeyersons, J., Deckers, J., Haile, M., and Lang, A.: Human impact on the environment in the Ethiopian and Eritrean highlands — A state of the art, Earth-Sci. Rev., 64, 273–320, https://doi.org/10.1016/S0012-8252(03)00078-3, 2004.

Palmer, W. C.: Meteorological Drought, Research Paper No. 45, U.S. Department of Commerce, Weather Bureau, Washington, DC, 1965.

Rhee, J., Im, J., and Carbone, G. J.: Monitoring agricultural drought for arid and humid regions using multi-sensor remote sensing data, Remote Sens. Environ., 114, 2875–2887, https://doi.org/10.1016/j.rse.2010.07.005, 2010.

Sandholt, I., Rasmussen, K., and Andersen, J.: A simple interpretation of the surface temperature/vegetation index space for assessment of surface moisture status, Remote Sens. Environ., 79, 213–224, https://doi.org/10.1016/S0034-4257(01)00274-7, 2002.

Segele, Z. T. and Lamb, P. J.: Characterization and variability of Kiremt rainy season over Ethiopia, Meteorol. Atmos. Phys., 89, 153–180, https://doi.org/10.1007/s00703-005-0127-x, 2005.

Seleshi, Y. and Zanke, U.: Recent changes in rainfall and rainy days in Ethiopia, Int. J. Climatol., 24, 973–983, https://doi.org/10.1002/joc.1052, 2004.

Sen, P. K.: Estimates of the regression coefficient based on Kendall's tau, J. Am. Stat. Assoc., 63, 1379–1389, https://doi.org/10.1080/01621459.1968.10480934, 1968.

Sheffield, J. and Wood, E. F.: Drought: Past Problems and Future Scenarios, Earthscan, London, 2011.

Teferi, E., Bewket, W., and Simane, B.: Effects of land use and land cover on selected soil quality indicators in the Upper Blue Nile basin of Ethiopia, Environ. Manage., 52, 405–421, https://doi.org/10.1007/s00267-013-0133-z, 2023.

Tesfaye, S., Birhane, E., Leijnse, T., and van der Zee, S. E. A. T. M.: Climatic controls of ecohydrological responses in the highlands of northern Ethiopia, Sci. Total Environ., 609, 551–562, https://doi.org/10.1016/j.scitotenv.2017.07.245, 2017.

Trenberth, K. E., Dai, A., van der Schrier, G., Jones, P. D., Barichivich, J., Briffa, K. R., and Sheffield, J.: Global warming and changes in drought, Nat. Clim. Change, 4, 17–22, https://doi.org/10.1038/nclimate2067, 2014.

Viste, E., Korecha, D., and Sorteberg, A.: Recent drought and precipitation tendencies in Ethiopia, Theor. Appl. Climatol., 112, 535–551, https://doi.org/10.1007/s00704-012-0746-3, 2013.

Wan, Z., Hook, S., and Hulley, G.: MOD11A2 MODIS/Terra Land Surface Temperature/Emissivity 8-Day L3 Global 1 km SIN Grid V006, NASA EOSDIS Land Processes DAAC, https://doi.org/10.5067/MODIS/MOD11A2.006, 2015.

Wang, C., Qi, S., Niu, Z., and Wang, J.: Evaluating soil moisture status in China using the Temperature/Vegetation Dryness Index (TVDI), Can. J. Remote Sens., 30, 671–679, https://doi.org/10.5589/m04-029, 2004.

Wei, T. and Simko, V.: R package corrplot: Visualization of a Correlation Matrix (Version 0.84), available at: https://github.com/taiyun/corrplot, 2017.

Wilhite, D. A. (Ed.): Drought: A Global Assessment, Routledge, London, 2000.

Wilhite, D. A., Sivakumar, M. V. K., and Pulwarty, R.: Managing drought risk in a changing climate: The role of national drought policy, Weather Clim. Extrem., 3, 4–13, https://doi.org/10.1016/j.wace.2014.01.002, 2014.

https://doi.org/10.5194/egusphere-2026-3534
Preprint. Discussion started: 20 July 2026

Woldesenbet, T. A., Elagib, N. A., Ribbe, L., and Heinrich, J.: Catchment response to climate and land use changes in the Upper Blue Nile sub-basins, Ethiopia, Sci. Total Environ., 644, 193–206, https://doi.org/10.1016/j.scitotenv.2018.06.198, 2023.

Yao, J., Mao, W., Yang, Q., Xu, X., and Liu, Z.: Annual actual evapotranspiration in inland mountain-basin areas: A case study in the Arid Central Asia, J. Geophys. Res. Atmos., 125, e2019JD031958, https://doi.org/10.1029/2019JD031958, 2020.

Yue, S. and Wang, C.: Applicability of prewhitening to eliminate the influence of serial correlation on the Mann-Kendall test, Water Resour. Res., 38, 4-1–4-7, https://doi.org/10.1029/2001WR000861, 2002.

Zhang, A., Jia, G., and Wang, H.: Improving meteorological drought monitoring capability over tropical and subtropical water-limited ecosystems: Validation and application of a modified satellite-based drought index, Environ. Res. Lett., 12, 044009, https://doi.org/10.1088/1748-9326/aa6a4e, 2017.